Title Page

Microthrombi-growth in ADAMTS13 deficiency exacerbated ulcerative colitis via mucosal and endothelial dysfunction

Kyota Tatsuta[1,2], M.D., Naoki Honkura[1,3,7], Ph.D., Nanami Morooka[1], Ph.D., Mayu Sakata[2], Ph.D., Kiyotaka Kurachi[2], Ph.D., Ken Sugimoto[4], Prof., Koichi Kokame[5], Ph.D., Hiroya Takeuchi[2], Prof., Tetsumei Urano[1,6], Ph.D., Yuko Suzuki[1], Prof.,

[1]Department of Medical Physiology, Hamamatsu University School of Medicine, Hamamatsu, Japan.

[2]Department of Surgery, Hamamatsu University School of Medicine, Hamamatsu, Japan.

[3]Multidimensional Imaging Laboratory, Institute of Photonics Medicine, Hamamatsu University School of Medicine, Hamamatsu, Japan.

[4]Department of Internal Medicine 1, Hamamatsu University School of Medicine, Hamamatsu, Japan.

[5]Department of Molecular Pathogenesis, National Cerebral and Cardiovascular Center, Suita, Osaka, Japan.

18 [6]Shizuoka Graduate University of Public Health, Shizuoka, Japan.

19 [7]PRESTO, Japan Science and Technology Agency, Tokyo, Japan.

20

21 **Short Title**

22 Microthrombi-growth worsens ulcerative colitis

23

24 **Corresponding authors:**

25 Yuko Suzuki and Naoki Honkura

26 Department of Medical Physiology, Hamamatsu University School of Medicine,

27 1-20-1, Handayama, Chuo-ku, Hamamatsu, 431-3192, Japan

28 Email: seigan@hama-med.ac.jp and pon@hama-med.ac.jp

29 Tel: +81-53-435-2248

30 FAX: +81-53-435-7020

31

32 **Total word count**

33 7334 words

Abstract

Background:

Ulcerative colitis (UC) is a chronic inflammatory bowel disease characterized by mucosal inflammation and ulceration, with systemic immune dysregulation exacerbating disease progression. While the accumulation of von Willebrand factor (VWF), normally digested by a disintegrin-like and metalloproteinase with thrombospondin type 1 motif 13 (ADAMTS13) from ultra-large multimers to small molecules, has been implicated in UC pathogenesis, the association between aberrant microthrombus formation and colitis remains unclear.

Methods:

Plasma and inflamed colonic tissues from UC patients were analyzed. In the experimental colitis model, we employed an intravital imaging technique to reveal real-time structural dynamics of the mucus layer and the mucosal vasculature. Dextran sulfate sodium (DSS)-induced colitis in wild-type and ADAMTS13-deficient mice was evaluated for disease progression, mucus layer disruption, leukocyte recruitment, and thrombus formation in mucosal vessels using intravital multiphoton excitation microscopy within single-cell spatial resolution.

Results:

UC patients exhibited significantly reduced plasma ADAMTS13 activity correlating with disease severity and excessive VWF deposition in inflamed colonic tissues. In DSS-induced colitis mice, ADAMTS13 deficiency showed heightened disease activity and increased mucosal erosion in histochemical analysis compared to wild-type mice. A novel methodology established in this study using intravital microscopy successfully appraised colonic mucus barrier integrity by visualizing fluorescent dextran penetration from the colonic lumen to the crypts. ADAMTS13 deficiency accelerated mucus layer disruption, leukocyte adhesion, and microthrombi formation, particularly close to crypt epithelium regions. Vessel-specific analyses demonstrated that obstructive microthrombi were most prominent in the mucosal layer, contributing to local ischemia and mucosal erosion. Therapeutical usage of recombinant human ADAMTS13 alleviated microthrombus formation, improved mucosal integrity, and mitigated colitis severity in wild-type and ADAMTS13-deficient mice.

Conclusions:

Obstructive thrombi formed in mucosal vessels due to impaired ADAMTS13 activity appeared essential in the disease progression of UC. Advanced intravital imaging provided novel insights into single-cell resolution UC pathogenesis.

67 **Non-standard Abbreviations and Acronyms**

68 UC, ulcerative colitis; VWF, von Willebrand factor; ADAMTS13, a disintegrin-like and
69 metalloproteinase with thrombospondin type 1 motif 1; UL, ultra-large; rhADAMTS13,
70 recombinant human ADAMTS13; GFP, green fluorescent protein; DSS, dextran sulfate sodium
71 DSS; PAS, periodic acid Schiff; TRITC, tetramethylrhodamine; ROI, regions of interest

72

73 **Introduction**

74 Ulcerative colitis (UC) is an inflammatory bowel disease that is characterized by inflammation
75 and mucosal ulceration that extends from the rectum to the colon.[1] The early stages of
76 pathogenesis in UC involve disruption of the mucus layer, which comprises goblet cell
77 secretory components, consequently the loss of mucosal homeostasis.[2] Subsequently, the
78 dysregulated activation of the mucosal immune system exacerbates colonic mucosal
79 inflammation and leads to the progression of systemic inflammation.[3] Despite significant
80 advancements in therapeutics through the utilization of molecularly targeted drugs that are
81 based on immune signals,[4] clinical trials continue to demonstrate low remission rates.[5,6] A
82 comprehensive understanding of the intricate pathophysiological mechanisms that both initiate
83 and exacerbate UC, including mucus layer disruptions and inflammatory responses within the
84 mucosal microvasculature, is crucial for enhancing disease management strategies.[7]

85 In these responses, von Willebrand factor (VWF) has emerged as a significant factor, closely
86 associated with endothelial dysfunction in UC.[8] A disintegrin-like and metalloproteinase with
87 thrombospondin type 1 motif 13 (ADAMTS13) cleaves ultra-large (UL)-VWF multimers,
88 which are stored in the Weibel-Palade bodies of endothelial cells and released into the blood in
89 response to various stimuli, into smaller and less reactive fragments with blood flow.[9]
90 Inflammatory diseases inhibit ADAMTS13 synthesis via inflammatory cytokines (e.g.,
91 interleukin-6 and tumor necrosis factor-α) and inactivate ADAMTS13 through proteases

92 released from neutrophils during inflammation,[10] resulting in the inability to cleave UL-VWF
93 multimers and potentially triggering thrombus formation. Clinical studies have suggested that
94 decreased ADAMTS13 activity is associated with an increased risk of thromboembolic events
95 in patients with UC.[11]

96 A previous study using UC model mice and human tissue sections revealed that ADAMTS13
97 deficiency led to VWF-rich thrombus formation in submucosal vessels, then exacerbating
98 colitis.[12] The administration of recombinant human ADAMTS13 (rhADAMTS13) reduced the
99 severity of colitis, suggesting its potential as an adjunct to existing therapies.[12] The presence of
100 thrombi in mucosal microvessels has been reported in several studies analyzing rectal biopsies
101 of patients with UC.[13,14] However, these findings remain inconclusive, as pathological analyses
102 were conducted exclusively on colon tissue sections. Consequently, the causal relationship
103 between microvessel thrombi and disease severity has yet to be established. Accurately
104 identifying the spatial and temporal distribution of thrombi within mucosal vessels during UC
105 progression significantly enhances the understanding of the underlying pathophysiological
106 mechanisms.

107 In decades, advances in real-time imaging techniques have enabled not only in vitro analyses
108 [15–17] but also the study of tissue in living animals,[18–21] allowing us to assess the spatiotemporal
109 dynamics in single platelets and vascular endothelial cells. We investigated the spatiotemporal
110 processes of platelet activation, coagulation, and fibrinolysis by employing a laser-induced

111 model of single endothelial cell injury in mice.[19–21] Advanced live imaging techniques utilizing
112 multiphoton excitation microscopy were further developed to achieve high spatial resolution,
113 thereby enabling the observation of individual cell dynamics.[22]

114 In this study, we employed low-invasive intravital imaging with multiphoton excitation
115 microscopy to investigate colonic lesions in colitis mice and attempted to elucidate the
116 spatiotemporal regulatory mechanisms that exacerbate colitis. We propose potential linkages
117 among mucus layer dysfunction, the increased formation of obstructive thrombi in the mucosal
118 microvessels near the epithelial layer, and the progression of disease, utilizing an ADAMTS13-
119 deficient microthrombosis model in mice.

120

121 **Methods**

122 Details can be found in the Supplemental Materials.

123 **Human sample preparations and analysis**

124 Ethical approval for using human samples was obtained from the IRB of Hamamatsu
125 University School of Medicine (approval no. 21-208). We obtained plasma and measured
126 plasma ADAMTS13 activity in samples from patients with UC and healthy volunteers.
127 Immunohistochemical analysis of VWF staining was conducted to compare the most inflamed
128 regions of UC tissues with the normal colon, defined in this study as non-cancerous areas from

129 Stage 0 or I colorectal cancer specimens.

130

131 **Animals**

132 The green fluorescent protein (GFP)-expressing transgenic C57BL/6J mice were supplied by
133 Dr. Okab.[23] *Adamts13*-deficient mice (C57BL/6 strain background) with confirmed activity
134 deficiency due to the lack of cleavage of GST-mVWF73-H and FRETS-VWF73, which are
135 specific substrates of ADAMTS13,[24] were crossed with GFP mice (ADAMTS13-KO mice).[21]
136 All experiment animals were 7- to 8-week-old males and weighed between 20 and 23 g. Age-
137 stratified data on body weight, autoclaved water consumption, and food intake are shown in
138 Figure S1. After the completion of the experiments, all mice were euthanized to minimize
139 unnecessary suffering.

140

141 **Dextran sulfate sodium-induced colitis mouse model**

142 Acute colitis was induced by the oral administration of 5% (w/v). DSS (MP Biomedicals) in
143 autoclaved water for 5 days. Daily weight and clinical colitis scores were measured using the
144 disease activity index[25] based on weight loss (0: none, 1: 1–5%, 2: 5–10%, 3: 10–15%, and 4:
145 >15%), stool consistency (0: normal, 2: loose stool, 4: watery diarrhea). and the degree of
146 intestinal bleeding (0, normal; 2, slight bleeding; and 4, gross bleeding).

147

148 **Histological assessment in the DSS-induced colitis mouse**

149 We evaluated inflammation-associated histological changes in the colon, the number and
150 length of the mucosal erosions, and the number of periodic acid Schiff (PAS)-positive goblet
151 cells per colonic crypt.

152

153 **Intravital imaging system**

154 Intravital imaging was conducted using a Nikon A1R MP multiphoton microscope (Nikon)
155 equipped with an ultrashort-pulse tunable Ti:sapphire laser (Chameleon Vision II, Coherent).
156 For two-photon excitation, wavelengths were set to either 960 nm or 1040 nm, tailored to each
157 experimental condition. Emitted fluorescence signals were split sequentially into green and red
158 channels via dichroic mirrors (560 nm and/or 593 nm), optimizing for each excitation
159 wavelength and fluorescence molecule brightness to prevent cross-talk. The fluorescence was
160 then filtered through band-pass emission filters (525/50 nm for green [GFP] and 629/56 nm for
161 red [TRITC: Tetramethylrhodamine or Alexa Fluor 568]) and captured separately using GaAsP
162 photomultiplier tubes.

163

164 **Recombinant human ADAMTS13 treatment**

165 A single shot of 0.5 μg RhADAMTS13 (R&D Systems) was administered by retro-orbital
166 intravenous injection every 24 h on days 1–5 after DSS administration. All experiments were
167 performed four hours after rhADAMTS13 administration.

168

169 **Results**

170 **Impaired ADAMTS13-VWF axis correlates with disease severity in UC**

171 First, we evaluated the effect of the ADAMTS13-VWF axis in patients with moderate-to-severe
172 UC, with disease severity defined according to the Endoscopic Mayo Score (Supplemental
173 methods for detailed classification).[26] In blood samples collected from patients with moderate-
174 to-severe UC before administering inpatient treatment, plasma ADAMTS13 activity levels
175 were significantly lower than in healthy controls (Figure 1A). Severe cases of UC showed
176 weaker ADAMTS13 activity than moderate cases, although the difference was not significant.
177 We undertook a detailed evaluation of the correlation between plasma ADAMTS13 activity
178 and plasma albumin levels, which are negatively correlated with disease progression, and
179 platelet counts, which are positively correlated with disease progression,[27] and found the
180 correlation of ADAMTS13 activities similar to the disease progression (Figure 1B and 1C). To
181 clarify how decreased ADAMTS13 activity affects VWF distribution in lesions, we performed
182 VWF staining in sections of inflammatory colon obtained from patients with UC. In normal

183 colon tissue sections, anti-VWF immunostaining showed VWF deposition only in the vessel
184 walls. In contrast, the inflamed tissue of patients with UC showed significant VWF
185 accumulation in the vessel walls and interstitial spaces of the mucosal and submucosal layers
186 (Figure 1D and 1E). We quantitatively analyzed the percentage of VWF-stained areas in the
187 mucosal and submucosal layers across the entire colonic tissue section. A significant increase
188 in VWF accumulation was observed in the inflamed UC colon compared to the normal colon
189 (Figure 1E). In addition, the amount of *VWF* mRNA in the colonic tissue of patients with active
190 UC was higher than that in the normal colon (Figure S2), which was analyzed using two
191 different datasets.[28,29] These results indicate that UC disease severity could be characterized by
192 the active levels of ADAMTS13 and VWF in inflamed lesions.

193

194 **ADAMTS13 deficiency exacerbates DSS-induced colitis in mice**

195 To understand the pathophysiological mechanism of colitis exacerbated by reduced
196 ADAMTS13 activity, we induced colitis in ADAMTS13-KO mice using DSS, which shows
197 many similarities with human UC.[30] Oral administration of 5% DSS induced similar weight
198 loss in WT and ADAMTS13-KO mice (Figure 2A), whereas the disease activity index, as
199 evaluated by weight loss, stool consistency, and the degree of intestinal bleeding, was more
200 severe in ADAMTS13-KO mice than in WT mice (Figure 2B). The high disease activity index

201 was mainly influenced by increased intestinal bleeding. After 5 days of DSS administration,
202 ADAMTS13-KO mice tended to show shorter colon lengths, a characteristic of DSS-induced
203 colitis in mice,[31] compared to WT mice (Figure 2C). Mucosal erosion in pathological colon
204 sections was more common in the ADAMTS13-KO mice with DSS-induced colitis than in the
205 WT mice (Figure 2D, black arrowheads). Histopathological scores, evaluated by the degree of
206 tissue damage and inflammatory cell infiltration,[31] were significantly higher in ADAMTS13-
207 KO mice with DSS-induced colitis (Figure 2E). The total number of mucosal erosions (Figure
208 2F) and the normalized length of mucosal erosion (Figure 2G) in the entire colon were
209 significantly increased in ADAMTS13-KO mice than in WT mice. Our findings indicate that
210 ADAMTS13 deficiency significantly exacerbates DSS-induced colitis, particularly at sites of
211 mucosal erosion in mice.

212

213 **Intravital imaging analysis of mucus layer barrier function**

214 To investigate the early-phase dynamics of UC pathophysiology, particularly concerning the
215 barrier function of the mucus layer (<1-μm thickness), we employed intravital imaging using
216 multiphoton excitation microscopy with fluorescent molecules. The colonic mucus layer
217 comprises a dual-layer system: a densely packed inner layer firmly attached to the epithelium
218 and a fluidic outer layer serving as a protective filter that physically separates bacteria from

219 epithelial cells.[32] By administering fluorescent dyes into the colon lumen, we attempted to
220 visualize the barrier function of the mucus layer, wherein the fluid mucus dynamics are usually
221 undeterminable with traditional biological methods. TRITC-dextran (40 kDa), a typical
222 biomolecular weight, was injected into the lumen to evaluate its distribution across the colonic
223 crypts, highlighting changes as the mucus layer progressively degraded under UC conditions.
224 After 15 minutes, the colonic lumen was adequately filled with TRITC-dextran, and images of
225 the mouse's proximal colon were captured by fixing it with agarose onto a glass slide (Figure
226 3A). TRITC-dextran (red) penetrated the lower parts of the crypts in WT mice with colitis on
227 day 5 post-DSS administration, contrasting with WT mice without colitis, where no such
228 penetration was observed (Figure 3B; Figure S3A; video S1 and S2). To quantify TRITC-
229 dextran distribution, regions of interest (ROIs) were set within the colonic crypts (Figure S3A),
230 and the red signal to the background (green channel) ratio was determined to account for inter-
231 individual variability. The stable GFP fluorescence originated from cells that drove a modified
232 chicken β-actin promoter in the GFP mice.[23] Notably, cells of the same type exhibited highly
233 consistent GFP expression levels across different individuals. This consistency allowed us to
234 use green fluorescence as a constant reference, enabling precise determination of the red-to-
235 green intensity ratio. By normalizing the red intensity to this stable green fluorescence, we
236 corrected for variability due to interindividual differences among mice and minor imaging
237 fluctuations, such as laser power variations along the z-axis (Figure 3B).

238

239 **Impact of ADAMTS13 deficiency on fluidic mucus layer barrier function**

240 The TRITC-dextran fluorescence baseline ratio (day 0) was established for WT mice pre-DSS
241 administration (Figure S3C). The DSS exposure increased fluorescence at both the lower and
242 upper crypt regions in WT and ADAMTS13-KO mice, indicating barrier permeability changes
243 (Figure S3B and S3C). Across all observed points, fluorescence in the upper crypt consistently
244 exceeded that of the lower part, regardless of genotypes (Figure 3C and 3D; Figure S3D).
245 Increased normalized fluorescence intensity on days 3 and 4 in ADAMTS13-KO mice,
246 alongside enhanced disease activity and histological damage, suggested a deficiency-
247 associated reduction in fluidic mucus layer integrity. No significant crypt length differences
248 were observed between the two genotypes (Figure 3E). Together, these findings indicate a DSS-
249 induced expansion of TRITC-dextran distribution from the lumen toward the lower crypt part
250 due to diminished mucus, implicating ADAMTS13 deficiency in mucus layer reduction and
251 endothelial dysfunction at early stages post-DSS exposure.

252

253 **Reduction of fluidic mucus layer and goblet cells following DSS administration**

254 We further assessed the correlation between TRITC-dextran penetration and goblet cell
255 depletion in the proximal colon. Reduced mucus secretion is known to correlate with a decrease

256 in goblet cell count.[33] To assess this, we evaluated goblet cells in the proximal colon using
257 intravital imaging, excluding regions of mucosal erosion. The number of goblet cells (PAS-
258 positive cells) within colonic crypts was determined by averaging counts from 10 crypts and
259 normalizing them to a surface area of 100 μm² per crypt. DSS administration resulted in a time-
260 dependent reduction of goblet cells in both genotypes (Figure 3F and 3G; Figure S4A).
261 However, no significant differences in goblet cell numbers were noted between genotypes on
262 days 3 and 4 post-DSS administration (Figure 3G). These observations suggest that DSS-
263 induced damage to goblet cells, accompanied by endothelial dysfunction, may impair mucus
264 release, impacting both cell counts and mucus volumes in colonic crypts. This assessment,
265 however, presents technical challenges without our novel TRITC-dextran-based methodology
266 (Figure 3C, 3D, and 3G; Figure S4A). A negative correlation was found between normalized
267 fluorescence intensity at the crypt's lower and upper and goblet cell count, which correlated
268 with DSS exposure duration (Figure 3H; Figure S4B and S4C).

269

270 **ADAMTS13 deficiency enhances leukocyte recruitment in DSS-induced colitis**

271 Disruption of the intestinal barrier promotes inflammatory cytokine production and immune
272 cell recruitment to the bowel wall.[34] We continuously examined early-stage events in DSS-
273 induced colitis, focusing on the subepithelial region and mucosal microvessels. To elucidate

274 the spatiotemporal remodeling of mucosal microvessels through inflammation, we observed
275 leukocyte rolling and adhesion in the microcirculation using high-spatiotemporal resolution
276 intravital imaging. Leukocytes, identified as GFP-positive cells (~10 μm, white arrows in
277 Figure S5A and S5B; video S3 through S6), were tracked in the circulation. From day 4 of DSS
278 treatment, WT mice displayed increased leukocyte rolling in both small vessels (10–50 μm,
279 Figure S6A) and larger vessels (>50 μm, Figure S6B). Notably, both genotypes of mice
280 exhibited enhanced leukocyte rolling and adhesion to the endothelial wall on day 5, but this
281 increase emerged earlier, from day 3, in ADAMTS13-KO mice (Figure S5C through S5F;
282 Figure S6). These results suggest that ADAMTS13 deficiency accelerates leukocyte
283 recruitment resulting from UL-VWF multimer-related endothelial response, then impacts
284 microcirculatory changes in the inflamed intestine during diminished mucus integrity.

285

286 **ADAMTS13 deficiency promotes microthrombus formation within mucosal and**
287 **submucosal vessels in DSS-induced colitis**

288 Activated endothelial cells by inflammation in the intestinal microvasculature, alongside
289 immune responses, could play a critical role in the early stages of UC. We investigated the
290 impact of endothelial cell-released VWF and the presence or absence of ADAMTS13 on
291 platelet adhesion and microthrombus formation within DSS-induced inflammatory lesions in

292 the mucosal and submucosal vessels. By using Alexa Fluor-568-labeled anti-VWF antibodies,
293 we imaged VWF within inflamed vessels and observed platelet adhesion to one or two layers
294 of VWF multimers (width < 10 μm) and microthrombi formed by aggregated platelets (width
295 ≥ 10 μm) (Figure 4A), similar to the images reported in the previous study.[21] Grossly, on day
296 5 post-DSS administration, microthrombi were larger and more prominent in ADAMTS13-KO
297 mice than in WT mice (Figure 4B, white arrows; video S7 and S8).

298 To compare microthrombus formation between WT and ADAMTS13-KO mice, we analyzed
299 1 × 1 mm image field for quantified microthrombi number and length from days 0 to 5 of DSS
300 administration. WT mice showed an increase in both parameters on day 5, though to a limited
301 extent (Figure 4C and 4D). In contrast, ADAMTS13-KO mice demonstrated earlier and more
302 extensive microthrombus formation than WT mice with a significant increase from day 4
303 (Figure 4E-H). A vessel diameter analysis showed that WT mice primarily exhibited small-
304 vessel microthrombi (10–50 μm; Figure S7A and S7C), whereas ADAMTS13-KO mice
305 exhibited widespread microthrombi across vessels of all diameters (Figure S7). These results
306 suggest that ADAMTS13-KO mice experience limited cleavage of endothelial cell-released
307 UL-VWF multimers, triggering increased platelet aggregation and accelerated microthrombus
308 formation in the mucosal and submucosal vasculature. Moreover, leukocyte recruitment was
309 notably enhanced in ADAMTS13-KO mice, particularly in small vessels, as demonstrated by
310 increased rolling counts (Figure S6A and S6C), suggesting a potential link to diminished mucus

311 production from the luminal side.

312

313 **Microthrombi in mucosal regions disrupt microcirculation and exacerbate colitis**

314 To explore the impact of microthrombi on colitis progression, we analyzed their distribution
315 within mucosal and submucosal vessels in ADAMTS13-KO mice. We first categorize regional
316 specificity based on their anatomical locations into three regions: the lower part of the crypt
317 (Area I), intermediate regions (Area II), and submucosa (Area III) (Figure 5A; Figure S8A).
318 The submucosal vessels, primarily consisting of arteries and veins, are larger, with diameters
319 exceeding 40 μm. Vessel diameters gradually decrease toward the lower part of the crypt
320 (Figure 5B).

321 Microthrombi (< 10 μm width) were detected in vessels across all areas by day 3, with the
322 highest prevalence in Area I, where their presence persisted over time (Figure 5C through 5E).
323 Larger microthrombi (≥ 10 μm width) first appeared in Area I on day 3 and increased markedly
324 by day 5 (Figure 5C), with a moderate presence in Area II (Figure 5D). In contrast, Area III
325 showed minimal microthrombus formation, which remained low throughout the observation
326 period (Figure 5E). These area-specific differences were consistent with vessel diameter
327 classifications shown in Figure S8.

328 Microthrombi formed in the lower part of the crypt contributes to impaired local blood flow,

329 resulting in mucosal microcirculatory disturbances and potential ischemia. Thrombi that
330 occupy more than 70% of the vessel diameter can significantly restrict or occlude blood flow,
331 as predicted by the Hagen–Poiseuille equation and demonstrated in the previous report.[35]
332 Stenosis rates were assessed by comparing the largest microthrombus width to the vessel
333 diameter across Areas I–III (Figure 5F). Microthrombi with a stenosis rate ≥70% were observed
334 in Area I beginning on day 4, with a significant increase by day 5 (Figure 5G). No similar
335 increase was noted in Areas II or III (Figure 5H and 5I). These findings indicate that obstructive
336 microthrombi in the lower part of the crypts exacerbate microcirculatory dysfunction,
337 potentially leading to epithelial ischemia and mucosal erosion (Figure 2D, 2F, and 2G).

338

339 **rhADAMTS13 administration reduces microthrombus formation and ameliorates DSS-**
340 **induced colitis**

341 To assess the therapeutic efficacy of rhADAMTS13 in reducing microthrombus formation,
342 daily intravenous administration of rhADAMTS13 was performed in both genotypes of mice
343 during the early phase of DSS-induced colitis. Treatment with rhADAMTS13 significantly
344 improved disease activity (Figure S9B), reduced mucosal erosion (Figure S9D and S9E), and
345 decreased microthrombus formation on day 5 (Figure 6A and 6B). Detailed regional analysis
346 showed that rhADAMTS13 administration in ADAMTS13-KO mice markedly reduced

347 microthrombus formation in Areas I and II, particularly those with high stenosis rates (Figure
348 6C). Notably, no microthrombi with a stenosis rate ≥70% were observed in any region
349 following rhADAMTS13 treatment (Figure 6C). These findings indicate that rhADAMTS13
350 effectively suppresses microthrombus formation, improves colonic microcirculation, and
351 contributes to the resolution of mucosal erosion and overall colitis severity.

352

353 **Discussion**

354 In this study, we used advanced intravital imaging techniques with multiphoton excitation
355 microscopy to directly visualize events occurring within the mucosal layer during colitis. We
356 demonstrated for the first time that the early stages of colitis, beginning with mucus layer
357 dysfunction and microthrombus formation in the mucosal vessels, play a critical role in
358 exacerbating disease severity. The mucus layer loses its protective function after DSS
359 administration, with this loss progressing faster in ADAMTS13-KO mice than in WT mice.
360 Concurrently, microthrombi due to ADAMTS13 deficiency enlarge over time, leading to
361 stenosis, particularly in the vessels of the lower part of colonic crypts. This narrowing of the
362 vessels causes a microcirculatory dysfunction, exacerbating colitis. RhADAMTS13 effectively
363 suppresses microthrombus formation, thereby improving the severity of colitis. These findings
364 suggest that a deficiency in ADAMTS13 leads to microthrombus formation in the mucosal

365 vessels, contributing to the refractory nature of UC.

366 Minimally invasive direct visualization successfully revealed subtle changes in the early
367 stages of colitis pathogenesis. Previous studies of intravital intestinal imaging involved
368 intestinal incisions and other surgical procedures for imaging analysis preparation.[36,37]
369 Although these invasive procedures effectively mitigate intestinal peristaltic activity, which
370 interferes with imaging analysis, they may also introduce secondary or artificial effects in the
371 tissues and microcirculation. Our approach, using only agarose fixation without intestinal
372 incision, enabled rigorous observation of the functional mucus layer and intestinal
373 microcirculation, allowing for the first-time evidence of microthrombi's involvement in early-
374 stage UC pathogenesis.

375 Detailed observation of the functional mucus layer by TRITC-labeled dextran intrusion from
376 the lumen to the epithelium enabled the early detection of alterations following the DSS
377 administration to induce experimental colitis. The mucus layer undergoes constant renewal
378 through mucin secretion from the goblet cells. The estimated mucus layer turnover duration in
379 live murine distal colonic tissue is 1–2 h.[38] Thus, in vivo assessment of the dynamic changes
380 within the mucus layer, characterized by pronounced fluctuations, is essential to elucidate the
381 pathogenic characteristics of early-stage UC. However, previous studies have evaluated the
382 mucus layer using fixed tissues with Carnoy's fixative solution[39] or ex vivo methods,[40] which
383 makes it challenging to analyze the fluctuating functional structure of mucus layers. Here, by

384 quantifying the distribution of fluorescent dextran in colonic crypts, we introduced a novel
385 approach for real-time functional assessment of the colonic mucus layer that enables the
386 identification of the onset of mucus layer dysfunction during colitis progression.

387 In UC, disruption of the mucus layer triggers a strong inflammatory response within the
388 intestinal epithelium.[4] We found that vessels in the lower part of the crypt were more
389 susceptible to thrombus formation than the area under the muscularis mucosae, i.e., the
390 submucosal area. A previous study showed that the aggregation of several aligned platelets
391 within vessels, in response to endothelial activation via topical application of Ca^{2+}, resulted in
392 progressive thrombus formation and eventual vascular occlusion.[41–43] This phenomenon was
393 particularly evident in ADAMTS13-KO mice. In our study, damaged colonic crypts in a colitis
394 pathology model of ADAMTS13-KO mice affected the mucosal vascular endothelium, leading
395 to aligned platelets, followed by the growth of microthrombi in the mucosal vessels, resulting
396 in severe stenosis exceeding 70%. Severe microthrombi-dependent stenosis could induce
397 microcirculatory dysfunction. Previous study has shown that ischemia and ischemia-
398 reperfusion injury lead to mucosal damage.[44] The absence of microthrombi causing severe
399 stenosis of over 70%, along with the significant improvement in mucosal erosion following
400 rhADAMTS13 administration, strongly supported this evidence. Hence, the ADAMTS13-
401 VWF system plays a significant role in the early stages of pathogenesis and contributes to its
402 exacerbation, depending on the severity of the inflammatory disease.

403 Recent findings highlight the crucial role of VWF in inflammation, where it recruits
404 leukocytes via direct or platelet-dependent interactions.[45] In vitro studies show VWF binding
405 to leukocyte P-selectin glycoprotein ligand-1 and β2-integrins,[46] mimicking interactions with
406 P-selectin and intercellular adhesion molecules for rolling and stable adhesion.[47] UL-VWF-
407 binding platelets indirectly support leukocyte recruitment by expressing p-selectin on their
408 activated surfaces under high shear stress.[48] Therefore, in addition to microcirculatory
409 dysfunction, we suggest that VWF-leukocyte interactions during mucosal microvascular
410 thrombus formation promote inflammatory cell recruitment to the colonic mucosa,
411 exacerbating colitis. This mechanism of microvascular thrombosis-induced organ damage is
412 implicated in conditions like deep vein thrombosis,[49] stroke,[50] and cardiovascular diseases.[51]

413 In conclusion, this study provides compelling evidence that the microthrombi formed at the
414 colonic mucosal vessels by insufficient ADAMTS13 activity contributes to exacerbating the
415 early stages of UC pathogenesis. Resolving circulatory dysfunction caused by microthrombus
416 formation is crucial for overcoming the refractory condition of UC.

417

418 **Acknowledgments**

419 Fluorescence imaging experiments were performed at the Advanced Research Facilities and
420 Services of the Hamamatsu University School of Medicine.

Sources of Funding

This work was supported by the JSPS KAKENHI [grant numbers JP22K16486 (M.S.) and JP22K08153 (Y.S.)], a Grant-in-Aid for Scientific Research (B) [grant number JP21H03352 (N.H.) and JP24K02857 (N.H.)], JST PRESTO [grant number JPMJPR19G9 (N.H.)], the Takeda Science Foundation (N.H.), and an HUSM Grant-in-Aid (K.T., N.H., Y.S.).

Disclosures

The authors declared no competing interests.

References

1. Ungaro R, Mehandru S, Allen PB, Peyrin-Biroulet L, Colombel JF. Ulcerative colitis. *Lancet*. 2017;389(10080):1756-1770. doi:10.1016/S0140-6736(16)32126-2

2. Van Der Post S, Jabbar KS, Birchenough G, Arike L, Akhtar N, Sjovall H, Johansson MEV, Hansson GC. Structural weakening of the colonic mucus barrier is an early event in ulcerative colitis pathogenesis. *Gut*. 2019;68(12):2142-2151. doi:10.1136/gutjnl-2018-317571

438 3. Neurath MF. Cytokines in inflammatory bowel disease. *Nat Rev Immunol*.
439 2014;14(5):329-342. doi:10.1038/nri3661

440 4. Le Berre C, Honap S, Peyrin-Biroulet L. Ulcerative colitis. *Lancet*.
441 2023;402(10401):571-584. doi:10.1016/S0140-6736(23)00966-2

442 5. Sandborn WJ, Su C, Sands BE, D'Haens GR, Vermeire S, Schreiber S, Danese S, Feagan
443 BG, Reinisch W, Niezychowski W, Friedman G, Lawendy N, Yu D, Woodworth D,
444 Mukherjee A, Zhang H, Healey P, Panés J. Tofacitinib as induction and maintenance
445 therapy for ulcerative colitis. *New Engl J Med*. 2017;376(18):1723-1736.
446 doi:10.1056/nejmoa1606910

447 6. Sands BE, Peyrin-Biroulet L, Loftus E V., Danese S, Colombel JF, Törüner M, Jonaitis
448 L, Abhyankar B, Chen J, Rogers R, Lirio RA, Bornstein JD, Schreiber S. Vedolizumab
449 versus adalimumab for moderate-to-severe ulcerative colitis. *New Engl J Med*.
450 2019;381(13):1215-1226. doi:10.1056/nejmoa1905725

451 7. Deban L, Correale C, Vetrano S, Malesci A, Danese S. Multiple Pathogenic Roles of
452 microvasculature in inflammatory bowel disease: A jack of all trades. *Am J Pathol*.
453 2008;172(6):1457-1466. doi:10.2353/ajpath.2008.070593

454 8. Stevens TRJ, James JP, Simmonds NJ, McCarthy DA, Laurenson IF, Maddison PJ,
455 Rampton DS. Circulating von Willebrand factor in inflammatory bowel disease. *Gut*.

456 1992;33(4):502-506. doi:10.1136/gut.33.4.502

457 9. Crawley JTB, de Groot R, Xiang Y, Luken BM, Lane DA. Unraveling the scissile bond:
458 how ADAMTS13 recognizes and cleaves von Willebrand factor. *Blood*.
459 2011;118(12):3212-3221. doi:10.1182/blood-2011-02-306597

460 10. Bernardo A, Ball C, Nolasco L, Moake JF, Dong JF. Effects of inflammatory cytokines
461 on the release and cleavage of the endothelial cell-derived ultralarge von Willebrand-
462 factor multimers under flow. *Blood*. 2004;104(1):100-106. doi:10.1182/blood-2004-01-
463 0107

464 11. Cibor D, Owczarek D, Butenas S, Salapa K, Mach T, Undas A. Levels and activities of
465 von Willebrand factor and metalloproteinase with thrombospondin type-1 motif, number
466 13 in inflammatory bowel diseases. *World J Gastroenterol*. 2017;23(26):4796-4805.
467 doi:10.3748/wjg.v23.i26.4796

468 12. Zitomersky N, Demers M, Martinod K, Gallant M, Cifuni S, Biswas A, Snapper S,
469 Wagner D. ADAMTS13 deficiency worsens colitis and exogenous ADAMTS13
470 administration decreases colitis severity in mice. *TH Open*. 2017;01(01):e11-e23.
471 doi:10.1055/s-0037-1603927

472 13. Dhillon AP, Anthony A, Sim R, Wakefield AJ, Sankey EA, Hudson M, Allison MC,
473 Pounder RE. Mucosal capillary thrombi in rectal biopsies. *Histopathology*.

474 1992;21(2):127-133. doi:10.1111/j.1365-2559.1992.tb00360.x

475 14. He G, Ouyang Q, Chen D, Li F, Zhou J. The microvacular thrombi of colonic tissue in
476 ulcerative colitis. *Dig Dis Sci*. 2007;52(9):2236-2240. doi:10.1007/s10620-006-9158-5

477 15. Suzuki Y, Mogami H, Ihara H, Urano T. Unique secretory dynamics of tissue
478 plasminogen activator and its modulation by plasminogen activator inhibitor-1 in
479 vascular endothelial cells. *Blood*. 2009;113:470-478. doi:10.1182/blood-2008-03

480 16. Suzuki Y, Yasui H, Brzoska T, Mogami H, Urano T. Surface-retained tPA is essential for
481 effective fibrinolysis on vascular endothelial cells. *Blood*. 2011;118(11):3182-3185.
482 doi:10.1182/blood-2011-05-353912

483 17. Brzoska T, Suzuki Y, Sano H, Suzuki S, Tomczyk M, Tanaka H, Urano T. Imaging
484 analyses of coagulation-dependent initiation of fibrinolysis on activated platelets and its
485 modification by thrombin-activatable fibrinolysis inhibitor. *Thromb Haemost*.
486 2017;117(04):682-690. doi:10.1160/TH16-09-0722

487 18. Falati S, Gross P, Merrill-Skoloff G, Furie BC, Furie B. Real-time in vivo imaging of
488 platelets, tissue factor and fibrin during arterial thrombus formation in the mouse. *Nat*
489 *Med*. 2002;8(10):1175-1180. doi:10.1038/nm782

490 19. Brzoska T, Tanaka-Murakami A, Suzuki Y, Sano H, Kanayama N, Urano T.
491 Endogenously generated plasmin at the vascular wall injury site amplifies lysine binding

492 site-dependent plasminogen accumulation in microthrombi. *PLoS One*.
493 2015;10(3):e0122196. doi:10.1371/journal.pone.0122196

494 20. Hayashi T, Mogami H, Murakami Y, Nakamura T, Kanayama N, Konno H, Urano T.
495 Real-time analysis of platelet aggregation and procoagulant activity during thrombus
496 formation in vivo. *Pflugers Arch*. 2008;456(6):1239-1251. doi:10.1007/s00424-008-
497 0466-9

498 21. Rybaltowski M, Suzuki Y, Mogami H, Chlebinska I, Brzoska T, Tanaka A, Banno F,
499 Miyata T, Urano T. In vivo imaging analysis of the interaction between unusually large
500 von Willebrand factor multimers and platelets on the surface of vascular wall. *Pflugers*
501 *Arch*. 2011;461(6):623-633. doi:10.1007/s00424-011-0958-x

502 22. Honkura N, Richards M, Laviña B, Sáinz-Jaspeado M, Betsholtz C, Claesson-Welsh L.
503 Intravital imaging-based analysis tools for vessel identification and assessment of
504 concurrent dynamic vascular events. *Nat Commun*. 2018;9(1):2746.
505 doi:10.1038/s41467-018-04929-8

506 23. Okabe M, Ikawa M, Kominami K, Nakanishi T, Nishimune Y. "Green mice" as a source
507 of ubiquitous green cells. *FEBS Lett*. 1997;407(3):313-319. doi:10.1016/S0014-
508 5793(97)00313-X

509 24. Banno F, Kokame K, Okuda T, Honda S, Miyata S, Kato H, Tomiyama Y, Miyata T.

510 Complete deficiency in ADAMTS13 is prothrombotic, but it alone is not sufficient to
511 cause thrombotic thrombocytopenic purpura. *Blood*. 2006;107(8):3161-3166.
512 doi:10.1182/blood-2005-07-2765

513 25. Kim JJ, Shajib MS, Manocha MM, Khan WI. Investigating intestinal inflammation in
514 DSS-induced model of IBD. *J Vis Exp*. 2012;(60):1-6. doi:10.3791/3678

515 26. Schroeder KW. Coated oral 5-aminosalicylic acid therapy for mildly to moderately
516 active ulcerative colitis. A randomized study. *N Engl J Med*. 1987;317(26):1625-1629.

517 27. Sands BE. Biomarkers of inflammation in inflammatory bowel disease.
518 *Gastroenterology*. 2015;149(5):1275-1285.e2. doi:10.1053/j.gastro.2015.07.003

519 28. Haberman Y, Karns R, Dexheimer PJ, Schirmer M, Somekh J, Jurickova I, Braun T,
520 Novak E, Bauman L, Collins MH, Mo A, Rosen MJ, Bonkowski E, Gotman N, Marquis
521 A, Nistel M, Rufo PA, Baker SS, Sauer CG, Markowitz J, Pfefferkorn MD, Rosh JR,
522 Boyle BM, Mack DR, Baldassano RN, Shah S, Leleiko NS, Heyman MB, Grifiths AM,
523 Patel AS, Noe JD, Aronow BJ, Kugathasan S, Walters TD, Gibson G, Thomas SD,
524 Mollen K, Shen-Orr S, Huttenhower C, Xavier RJ, Hyams JS, Denson LA. Ulcerative
525 colitis mucosal transcriptomes reveal mitochondriopathy and personalized mechanisms
526 underlying disease severity and treatment response. *Nat Commun*. 2019;10(1):38.
527 doi:10.1038/s41467-018-07841-3

528 29. Fenton CG, Taman H, Florholmen J, Sørbye SW, Paulssen RH. Transcriptional
529 signatures that define ulcerative colitis in remission. *Inflamm Bowel Dis*. 2021;27(1):94-
530 105. doi:10.1093/ibd/izaa075

531 30. Okayasu I, Hatakeyama S, Yamada M, Ohkusa T, Inagaki Y, Nakaya R. A novel method
532 in the induction of reliable experimental acute and chronic ulcerative colitis in mice.
533 *Gastroenterology*. 1990;98(3):694-702. doi: 10.1016/0016-5085(90)90290-h.

534 31. Wirtz S, Popp V, Kindermann M, Gerlach K, Weigmann B, Fichtner-Feigl S, Neurath
535 MF. Chemically induced mouse models of acute and chronic intestinal inflammation.
536 *Nat Protoc*. 2017;12(7):1295-1309. doi:10.1038/nprot.2017.044

537 32. Johansson ME V., Phillipson M, Petersson J, Velcich A, Holm L, Hansson GC. The inner
538 of the two Muc2 mucin-dependent mucus layers in colon is devoid of bacteria. *Proc Natl*
539 *Acad Sci U S A*. 2008;105(39):15064-15069. doi:10.1073/pnas.0803124105

540 33. Grootjans J, Hundscheid IHR, Lenaerts K, Boonen B, Renes IB, Verheyen FK, Dejong
541 CH, von Meyenfeldt MF, Beets GL, Buurman WA. Ischaemia-induced mucus barrier
542 loss and bacterial penetration are rapidly counteracted by increased goblet cell secretory
543 activity in human and rat colon. *Gut*. 2013;62(2):250-258. doi:10.1136/gutjnl-2011-
544 301956

545 34. Zhang D, Frenette PS. Cross talk between neutrophils and the microbiota. *Blood*.

546 2019;133(20):2168-2177. doi:10.1182/blood-2018-11-844555

547 35. Sato M, Ohshima N. Hemodynamics at stenoses formed by growing platelet thrombi in
548 mesenteric microvasculature of rat. *Microvasc Res*. 1986;31(1):66-76.
549 doi:10.1016/0026-2862(86)90007-5

550 36. Gustafsson JK, Davis JE, Rappai T, McDonald KG, Kulkarni DH, Knoop KA, Hogan
551 SP, Fitzpatrick JA, Lencer WI, Newberry RD. Intestinal goblet cells sample and deliver
552 lumenal antigens by regulated endocytic uptake and transcytosis. *Elife*. 2021;10;e67292.
553 doi:10.7554/eLife.67292

554 37. Sullivan DP, Bui T, Muller WA, Butin-Israeli V, Sumagin R. In vivo imaging reveals
555 unique neutrophil transendothelial migration patterns in inflamed intestines. *Mucosal*
556 *Immunol*. 2018;11(6):1571-1581. doi:10.1038/s41385-018-0069-5

557 38. Johansson ME V. Fast renewal of the distal colonic mucus layers by the surface goblet
558 cells as measured by in vivo labeling of mucin glycoproteins. *PLoS One*.
559 2012;7(7):e41009. doi:10.1371/journal.pone.0041009

560 39. Naama M, Telpaz S, Awad A, Ben-Simon S, Harshuk-Shabso S, Modilevsky S, Rubin
561 E, Sawaed J, Zelik L, Zigdon M, Asulin N, Turjeman S, Werbner M, Wongkuna S,
562 Feeney R, Schroeder BO, Nyska A, Nuriel-Ohayon M, Bel S. Autophagy controls mucus
563 secretion from intestinal goblet cells by alleviating ER stress. *Cell Host Microbe*.

564 2023;31(3):433-446.e4. doi:10.1016/j.chom.2023.01.006

565 40. Gustafsson JK, Ermund A, Johansson ME V, Schütte A, Hansson GC, Sjövall H. An ex
566 vivo method for studying mucus formation, properties, and thickness in human colonic
567 biopsies and mouse small and large intestinal explants. *Am J Physiol Gastrointest Liver*
568 *Physiol*. 2012;302:430-438. doi:10.1152/ajpgi.00405.2011.

569 41. Chauhan AK, Motto DG, Lamb CB, Bergmeier W, Dockal M, Plaimauer B, Scheiflinger
570 F, Ginsburg D, Wagner DD. Systemic antithrombotic effects of ADAMTS13. *J Exp Med*.
571 2006;203(3):767-776. doi:10.1084/jem.20051732

572 42. Adili R, Holinstat M. Formation and resolution of pial microvascular thrombosis in a
573 mouse model of thrombotic thrombocytopenic purpura. *Arterioscler Thromb Vasc Biol*.
574 2019;39(9):1817-1830. doi:10.1161/ATVBAHA.119.312848

575 43. Chauhan AK, Goerge T, Schneider SW, Wagner DD. Formation of platelet strings and
576 microthrombi in the presence of ADAMTS-13 inhibitor does not require P-selectin or
577 β3 integrin. *J Thromb Haemost*. 2007;5(3):583-589. doi:10.1111/j.1538-
578 7836.2007.02361.x

579 44. Ikeda H, Suzuki Y, Suzuki M, Koike M, Tamura J, Tong J, Nomura M, Itoh G. Apoptosis
580 is a major mode of cell death caused by ischaemia and ischaemia/reperfusion injury to
581 the rat intestinal epithelium. *Gut*. 1998;42(4):530-537. doi:10.1136/gut.42.4.530

582 45. Kawecki C, Lenting PJ, Denis C V. von Willebrand factor and inflammation. *J Thromb*
583 *Haemost*. 2017;15(7):1285-1294. doi:10.1111/jth.13696

584 46. Pendu R, Terraube V, Christophe OD, Gahmberg CG, De Groot PG, Lenting PJ, Denis
585 C V. P-selectin glycoprotein ligand 1 and β2-integrins cooperate in the adhesion of
586 leukocytes to von Willebrand factor. *Blood*. 2006;108(12):3746-3752.
587 doi:10.1182/blood-2006-03-010322

588 47. McEver R. Adhesive Interactions of Leukocytes, Platelets, and the Vessel Wall during
589 Hemostasis and Inflammation. *Thromb Haemost*. 2001;86(09):746-756. doi:10.1055/s-
590 0037-1616128

591 48. Bernardo A, Ball C, Nolasco L, Choi H, Moake JL, Dong JF. Platelets adhered to
592 endothelial cell-bound ultra-large von Willebrand factor strings support leukocyte
593 tethering and rolling under high shear stress. *J Thromb Haemost*. 2005;3(3):562-570.
594 doi:10.1111/j.1538-7836.2005.01122.x

595 49. Pagliari MT, Cairo A, Boscarino M, Mancini I, Pappalardo E, Bucciarelli P, Martinelli
596 I, Rosendaal FR, Peyvandi F. Role of ADAMTS13, VWF and F8 genes in deep vein
597 thrombosis. Miyata T, ed. *PLoS One*. 2021;16(10):e0258675.
598 doi:10.1371/journal.pone.0258675

599 50. Xu H, Cao Y, Yang X, Cai P, Kang L, Zhu X, Luo H, Lu L, Wei L, Bai X, Zhu Y, Zhao

600 BQ, Fan W. ADAMTS13 controls vascular remodeling by modifying VWF reactivity
601 during stroke recovery. *Blood*. 2017;130(1):11-22. doi:10.1182/blood-2016-10-747089

602 51. De Meyer SF, Savchenko AS, Haas MS, Schatzberg D, Carroll MC, Schiviz A, Dietrich
603 B, Rottensteiner H, Scheiflinger F, Wagner DD. Protective anti-inflammatory effect of
604 ADAMTS13 on myocardial ischemia/reperfusion injury in mice. *Blood*.
605 2012;120(26):5217-5223. doi:10.1182/blood-2012-06-439935

606

607 **Highlights**

608 Intravital imaging with single-cell resolution revealed mucosal structure disruption and area-
609 specific microthrombus formation in ulcerative colitis model.

610 ADAMTS13 deficiency enhances microvascular obstructive thrombi causing local ischemia
611 and mucosal erosion.

612 Advanced imaging techniques provid new insights into ulcerative colitis pathophysiology and
613 contribute to resolving the challenges of its refractory condition.

614

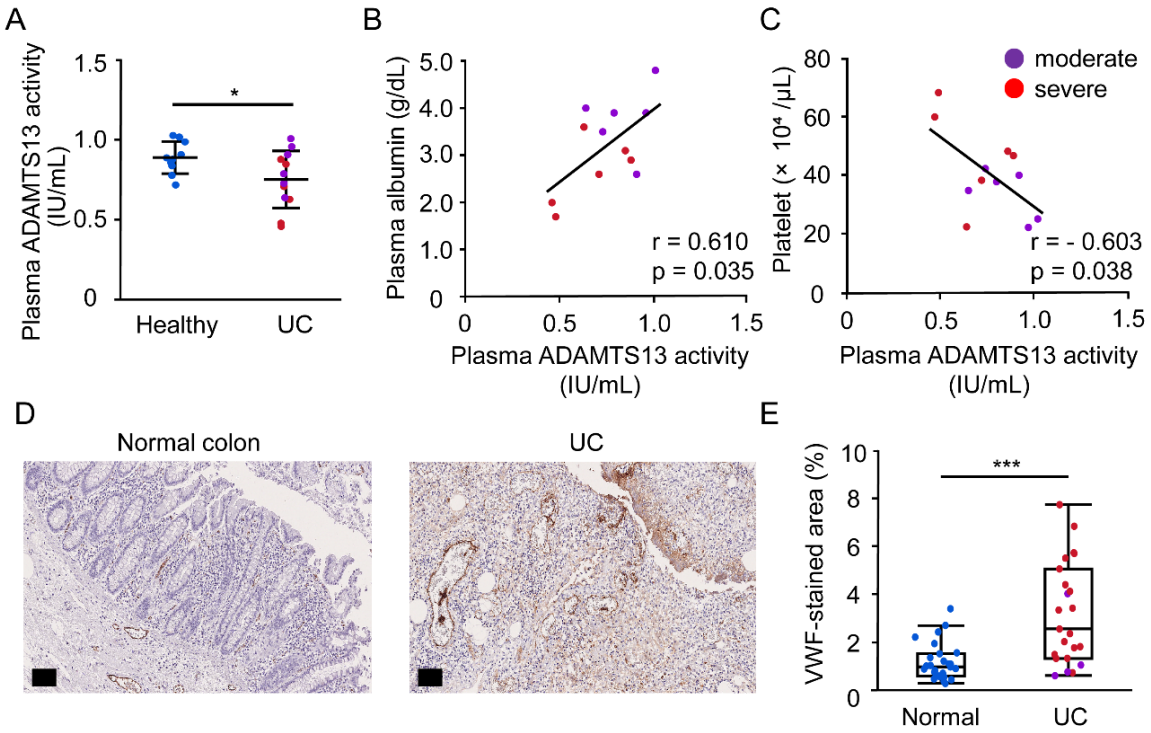

Figure 1. Decreased ADAMTS13 activity and increased VWF level in patients with UC

(A) Comparison of plasma ADAMTS13 activity in healthy controls (n=10, blue dots) and patients with UC (n=12). UC disease severity was defined as moderate and severe based on Endoscopic Mayo Scores of 2 and 3 (n=6 each, purple and red dots), respectively. (B, C) The relationship of plasma ADAMTS13 activity levels with plasma albumin levels and platelet counts in UC. (D) Representative images of VWF immunohistochemistry in colonic tissue sections from normal colon and those with UC; scale bar: 100 μm. (E) Quantitative analysis of VWF-stained areas in colonic surgical specimens from normal (n=27) and inflamed UC (n=24) participants. Data (A), presented as mean and SD, were analyzed by the Student's t-test. Data (B, C) were analyzed by the two-sided Spearman's correlation. Data (E), presented as median (center line) with 25th and 75th percentiles (box bounds) and whiskers (maximum and minimum data points), were analyzed by the Mann–Whitney U test. *p<0.05; ***p<0.001.

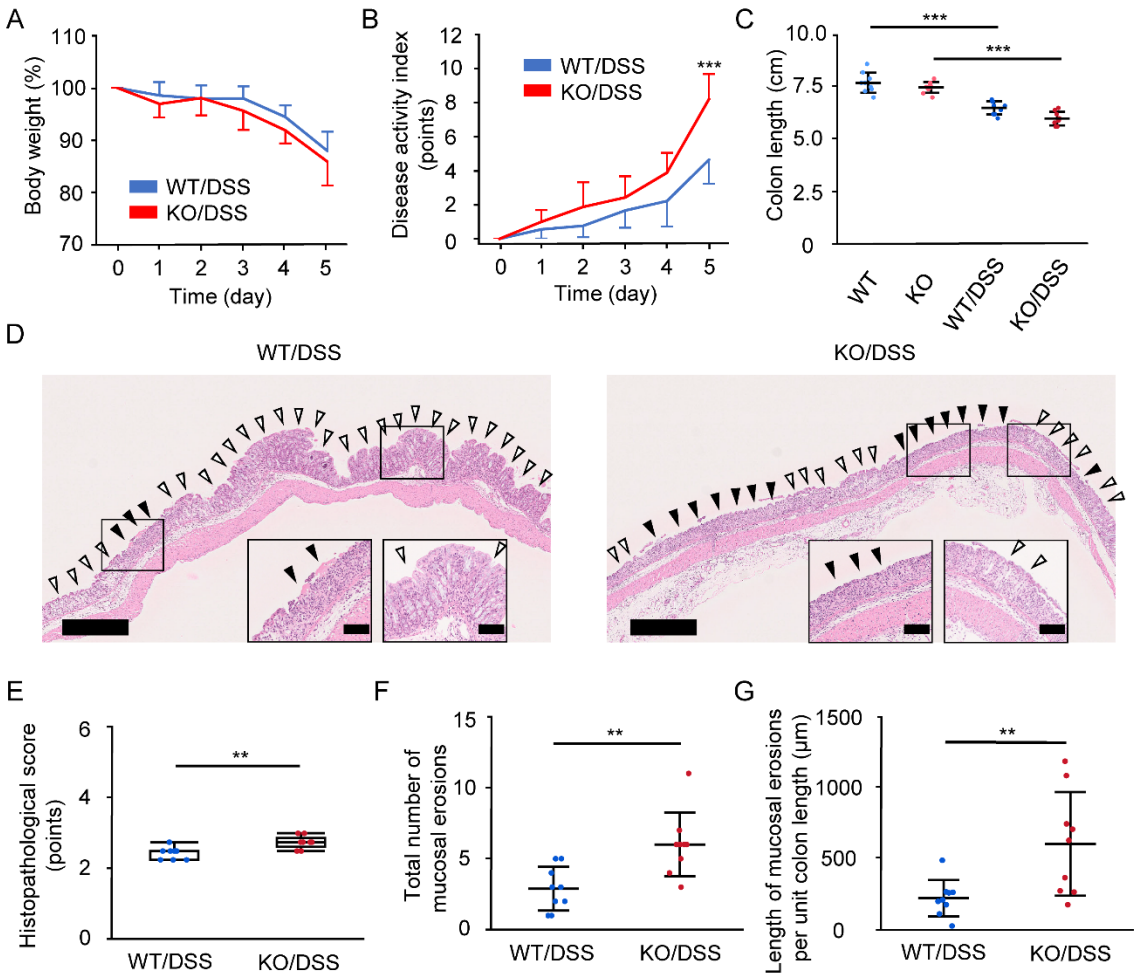

Figure 2. The impact of ADAMTS13 deficiency on DSS-induced colitis in mice

Mice (age: 7–8 weeks, male, n=9 per group) were administered 5% DSS for 5 days. (A, B) Changes in body weight and the disease activity index from 0 to 5 days (blue lines, WT mice; red lines, ADAMTS13-KO mice). (A) Body-weight changes are shown as percentages of those before DSS administration (day 0). (B) Disease activity indices (0, no symptoms, to 12, most severe) were calculated daily based on weight loss, stool consistency, and degree of intestinal bleeding. (C) The total colon length from the proximal colon to the rectum was measured on days 0 and 5 (light blue dots, WT mice on day 0; light red dots, ADAMTS13-KO mice on day 0; blue dots, WT mice on day 5; red dots, ADAMTS13-KO mice on day 5). (D) Representative images of H&E staining of DSS-induced inflamed colon sections of WT and ADAMTS13-KO mice on day 5 (black and white arrowheads: areas of mucosal erosion and where the surface epithelium is maintained, respectively; scale bars: 500 and 100 μm [inset]). (E) Histopathological scores (0, no inflammation, to 6, most severe inflammation) on day 5. (F) Number of mucosal erosions in the entire colon on day 5. (G) The length of mucosal erosions per 1 cm total colon length on day 5. Data presented as (A–C) mean and SD, analyzed by the Student's t-test with Bonferroni correction, (E) Median (center line) with 25th and 75th percentiles (box bounds) and whiskers (maximum and minimum data points), analyzed using the Mann–Whitney U test, and (F, G) mean and SD, analyzed using the Student's t-test. **p<0.01; ***p<0.001.

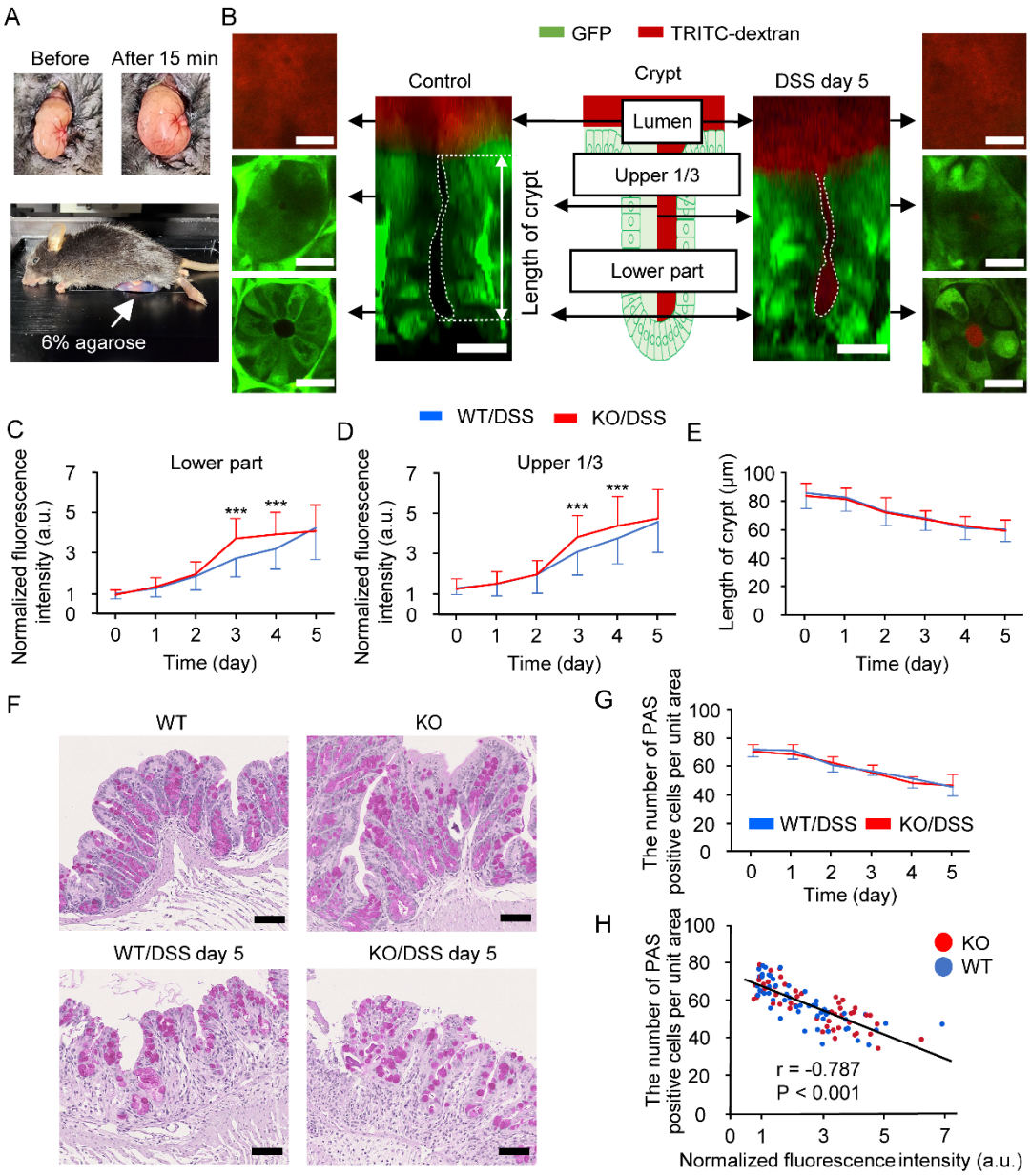

Figure 3. Functional evaluation of the colonic mucus layer

Mice (age: 7–8 weeks, male, n=9 per group) were administered 5% DSS for 5 days. (A) Proximal colon (fixed on 6% agarose) before and 15 min after dextran administration. (B) TRITC-dextran (red) distribution of colonic crypts in the control and DSS-induced colitis groups (day 5; scale bar: 20 μm). (C, D) Normalized fluorescence intensity of TRITC-dextran in the lower (C) and upper one-third (D) crypts. (E) Colonic crypt length (measured at the site indicated in B). (F) Representative images of periodic acid-Schiff (PAS) staining of proximal colon sections prepared from the intravital imaging area (goblet cells were stained purple; scale bar: 50 μm). (G) The number of PAS-positive cells per 100 μm2 of the crypts in DSS-induced WT (blue) and ADAMTS13-KO (red) mice. (H) Correlation between the normalized fluorescence intensity of TRITC-dextran in the lower part of the crypts and the number of goblet cells in the intravital imaging area. Data (mean ± SD) were analyzed by the Student's t-test with Bonferroni correction (C–E and G) and the two-sided Spearman's correlation (H). ***p<0.001.

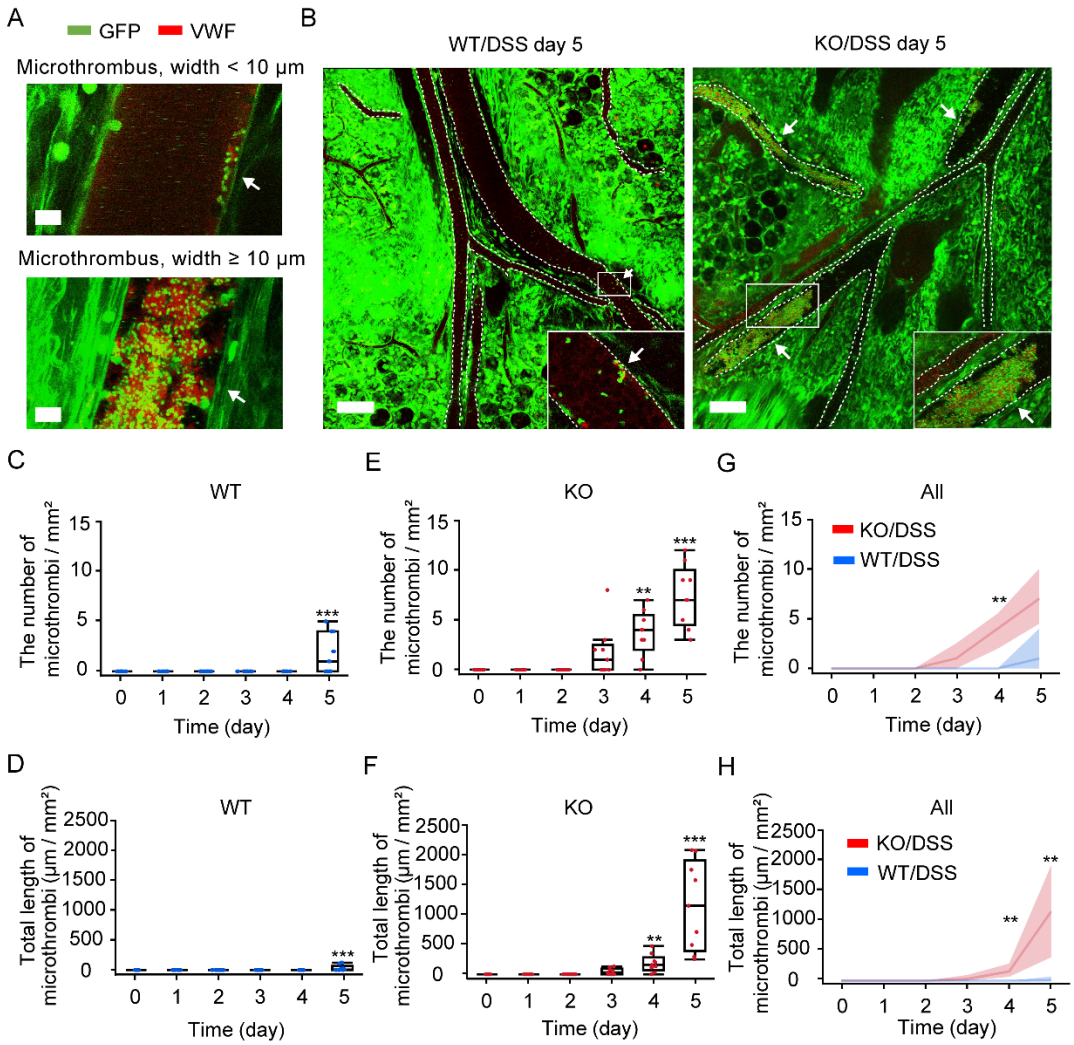

Figure 4. Microvascular thrombus formation in the colonic mucosal and submucosal area in DSS-induced colitis

Mice (age: 7–8 weeks, male, n=9 per group) were administered 5% DSS for 5 days. Thirty minutes before intravital observation, Alexa Fluor 568-labeled anti-VWF antibody was injected intravenously. (A) Representative images of microthrombus categorized by thrombus width. Green, GFP; red, anti-VWF antibody; scale bar: 10 μm (B) Representative images of microthrombi within mucosal and submucosal vessels of WT and ADAMTS13-KO mice 5 days after DSS administration (each inset shows the magnified image of the boxed region; white arrows, microthrombi with VWF accumulation; scale bar: 100 μm). (C, E, G) Changes over time in the number of microthrombi in WT mice (blue) (C), ADAMTS13-KO mice (red) (E), and both genotypes of mice (G) 0–5 days after DSS administration in a large observation area (1 × 1 mm field). (D, F, H) Changes in the total length of microthrombi in WT mice (blue) (D), ADAMTS13-KO mice (red) (F), and both genotypes of mice (H) at 0–5 days after DSS administration in a large observation area. Data (C–F) are shown as the median (center line), 25th and 75th percentiles (box bounds), and whiskers (maximum and minimum data points). Statistically significant changes were assessed using Steel's multiple comparison test to compare values recorded on day 0 with those on the other days. Data (G, H) are presented as a median and interquartile range, with statistical significance assessed using the Mann–Whitney U test with Bonferroni correction. **p<0.01; ***p<0.001.

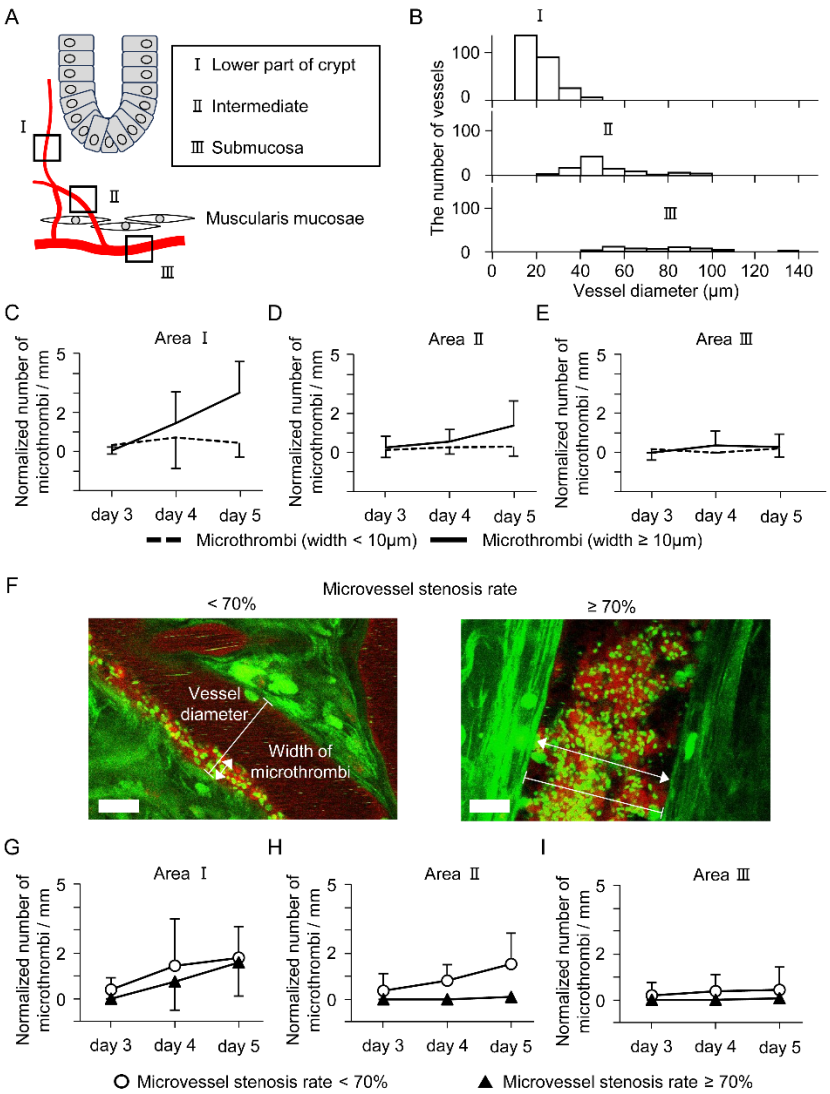

Figure 5. Spatiotemporal analysis of microthrombi in the mucosal and submucosal vessels

ADAMTS13-KO Mice (age: 7–8 weeks, male, n=9) were administered 5% DSS for 5 days, and all observed microthrombi were analyzed. (A) Microvascular anatomical classification of colonic crypts: a. the lower part of the crypt (Area I), b. intermediate area (Area II), c. submucosa (Area III). (B) Distribution of vessel diameters according to the anatomical classification of colonic epithelial. (C-E) Comparison of temporal changes in the normalized number of microthrombi at the 10 μm width boundary in vessels from Area I (C), Area II (D), and Area III (E). The number of microthrombi per millimeter was calculated by normalizing to the length of the blood vessel. Microthrombi with a width of ≥ 10 μm at Area I (C, black line) showed a significant increase over time ($p<0.001$). Microthrombi with the width < 10μm: dotted black line; microthrombi with the width ≥ 10μm: black line. (F) Calculation method for microvascular stenosis rate. Green, GFP; red, anti-VWF antibody scale bar: 10 μm. (G-I) Comparison of temporal changes in the normalized number of microthrombi at the 70% stenosis rate boundary in the vessels at Area I (G), Area II (H), and Area III (I). Microthrombi with stenosis rate ≥ 70% at Area I (G, black triangle) showed a significant increase over time ($p<0.01$). Stenosis rates less than 70%, white circle; 70% or more, black triangle. Data (C-E, G-I; mean ± SD) were analyzed by Dunnett's multiple comparison test to compare values recorded on day 3 with those on the other days.

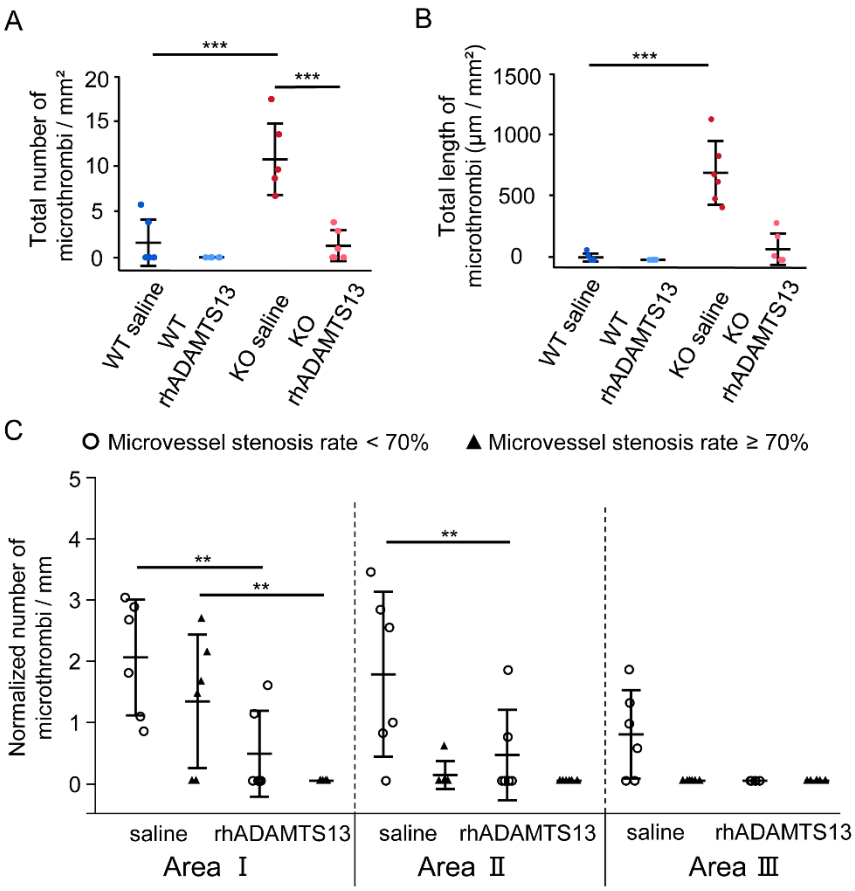

Figure 6. Improvement of mucosal and submucosal vascular microthrombi in DSS-induced colitis after rhADAMTS13 treatment

Mice (age: 7–8 weeks, male, n=6 per group) were administered 5% DSS for 5 days and simultaneously received rhADAMTS13 (WT, light blue dots; KO, light red dots) or saline (WT, blue dots; KO, red dots) injected intravenously on days 1–5. (A) Number of microthrombi on day 5. (B) Total length of microthrombi on day 5. (C) The normalized number of microthrombi on day 5 according to microvascular anatomical classification. Data (A-C; mean ± SD) were analyzed by the Student's t-test with Bonferroni correction. **p<0.01; ***p<0.001.